AGU PUBLICATIONS

JGR

Journal of Geophysical Research: Space Physics

RESEARCH ARTICLE
10.1002/2014JA020156

Key Points:
- Low-latitude ionospheric variability during prolonged southward IMF Bz
- The role of storm time equatorward, interhemispheric, and day-night winds
- Storm time thermospheric neutral composition variations

Correspondence to:
M. S. Bagiya,
bagiyamala@gmail.com

Citation:
Bagiya, M. S., R. Hazarika, F. I. Laskar, S. Sunda, S. Gurubaran, D. Chakrabarty, P. K. Bhuyan, R. Sridharan, B. Veenadhari, and D. Pallamraju (2014), Effects of prolonged southward interplanetary magnetic field on low-latitude ionospheric electron density, *J. Geophys. Res. Space Physics*, *119*, doi:10.1002/2014JA020156.

Received 5 MAY 2014
Accepted 13 JUN 2014
Accepted article online 16 JUN 2014

Effects of prolonged southward interplanetary magnetic field on low-latitude ionospheric electron density

Mala S. Bagiya[1], Rumajyoti Hazarika[2], Fazlul I. Laskar[3], Surendra Sunda[4], S. Gurubaran[1], D. Chakrabarty[3], P. K. Bhuyan[2], R. Sridharan[3], B. Veenadhari[1], and D. Pallamraju[3]

[1]Indian Institute of Geomagnetism, Navi Mumbai, India, [2]Department of Physics, Dibrugarh University, Dibrugarh, India, [3]Space and Atmospheric Sciences Division, Physical Research Laboratory, Ahmedabad, India, [4]Space Application Centre, Ahmedabad, India

Abstract The present work describes the low-latitude ionospheric variability during an unusually prolonged (~33 h) geomagnetically disturbed condition that prevailed during 15–16 July 2012. The low-latitude electron density in summer hemisphere, investigated using ground- and satellite-based observations, responded to this by generating strong negative ionospheric storm on 16 July. The maximum electron density on 16 July over Indian low latitudes was reduced by more than 50% compared to that on a geomagnetically quiet day (14 July 2012). In contrast to the extreme reduction in total electron content (TEC) in the Northern Hemisphere, TEC from a winter hemispheric station revealed substantial (~23 total electron content unit, 1 TECU = 10^{16} el m^{-2}) enhancements on the same day. This contrasting hemispherical response in TEC is suggested to be due to the combined effects of strong interhemispheric and solar-driven day-night winds. Further, very weak equatorial electrojet (EEJ) strength on 16 July indicated that the westward electric field perturbations in the low-latitude ionosphere were possibly due to the disturbance dynamo effect associated with meridional circulation from polar to equatorial latitudes. Interestingly, despite reduction in the integrated EEJ strength on 15 July, the low-latitude electron density showed substantial enhancement, highlighting the significant effect of the positive ionospheric storm on the low-latitude ionosphere. The roles of electrodynamical/neutral-dynamical and compositional disturbances are discussed in view of these observations to understand low-latitude ionospheric response when geomagnetic disturbance persists for longer duration.

1. Introduction

The storm time energy deposition at high latitudes is mainly determined by three processes: (i) the particle heating due to precipitation of auroral electrons and protons, (ii) the Joule heating due to relative motion of plasma and neutrals, and (iii) the ion drag. Among these, the Joule heating is now known to be the main atmospheric energy source during geomagnetic storms [*Fuller-Rowell et al*., 1996; *Kozyra et al*., 1998; *Mac-Mahon and Gonzalez*, 1997; *Sharber et al*., 1998; *Lu et al*., 1998]. Although the energy input takes place in both hemispheres, the responses of the northern and southern polar regions, corresponding to this energy input, are expected to differ. This is due to the solar illumination in the summer polar region which enhances the summer Joule heat source by more than 50% compared to that in the winter polar region [*Fuller-Rowell et al*., 1996]. The major source of Joule heating is the electric current caused due to the friction between neutrals and ions. The storm time-enhanced Joule heating at high latitudes changes the thermospheric wind circulation and neutral composition globally [e.g., *Fuller-Rowell et al*., 1996]. The excess energy deposition at high latitudes induce an equatorward meridional wind, and such a wind in conjunction with background diurnal and summer-to-winter interhemispheric winds redistributes thermospheric species globally. The storm time equatorward wind may get added coherently with the interhemispheric wind in the summer hemisphere, while the two would blow in opposite directions in the winter hemisphere. Thus, the storm effects might get extended to lower latitudes in the summer hemisphere while they would remain confined to the winter high latitudes [*Prölss*, 1976].

The storm-induced temperature enhances the upward vertical wind at high latitudes which would raise the molecular rich air in altitude and increase the thermospheric mean molecular mass there [*Immel et al*., 2001].

The equatorward wind also contributes in this increase by raising the molecular rich air upward during upwelling [*Rishbeth et al*., 1987; *Burns et al*., 1991]. The equatorward thermospheric wind along with the diurnal wind transports the enhanced mean molecular mass, the so-called "compositional bulge" [*Prölss*, 1980], toward middle to low latitudes [e.g., *Roble et al*., 1977; *Fuller-Rowell et al*., 1998. and references therein] where downward vertical wind would then lower the storm-induced upwelling. The neutral composition, in general, given by the ratio of atomic oxygen (O) to molecular species (N_2 and O_2), decreases at high latitudes during the upwelling and further increases at middle to low latitudes under the influence of downwelling during the early phase of a storm [e.g., *Rishbeth et al*., 1987; *Fuller-Rowell et al*., 1996; *Crowley et al*., 2006, and references therein]. The initial increase of [O/N_2] at low latitudes enhances the ionospheric electron density there (positive ionospheric storm) during the first few hours of the storm and reduces after around a day of the storm commencement (negative ionospheric storm) [e.g., *Burns et al*., 1995; *Strickland et al*., 2001; *Liou et al*., 2005; *Bagiya et al*., 2011]. The compositional bulge exhibits an apparent motion across day and night sectors [e.g., *Fuller-Rowell et al*., 1996] while moving toward lower latitudes. The storm-induced equatorward wind and solar-driven diurnal wind blow in opposite directions during daytime while in the same direction during nighttime. Therefore, transportation of the compositional bulge is more significant in the summer nighttime when winds are directed equatorward. It is known that the O and N_2 densities have a major role in the production and loss of the ionosphere, respectively. The photoionization of atomic oxygen is the main production process in the ionosphere while the recombination of electrons with ambient N_2^+ and O_2^+, through a two-step process, is the major chemical loss mechanism [*Rishbeth and Garriot*, 1969].

In addition to global neutral-dynamical changes which affect the ionospheric electron density distribution at low latitudes, the ionospheric electrodynamics also get modulated over middle to low latitudes due to the prompt penetration of storm time high-latitude electric field [*Spiro et al*., 1988; *Sastri et al*., 1997] and disturbance dynamo electric field after a delay [*Blanc and Richmond*, 1980]. Under the prompt penetration effect, the interplanetary electric field penetrates from high to low latitudes almost instantaneously with the starting of the main phase and perturbs the low-latitude ionospheric electric field within few minutes and up to an hour after the storm commencement. The penetration is usually eastward during daytime, thus enhancing the ionospheric electric field, and westward during nighttime. On the other hand, electric field perturbations associated with overshielding effects of interplanetary electric field are generally westward in the day sector [e.g., *Simi et al*., 2012] and eastward in the night sector [e.g., *Chakrabarty et al*., 2006]. Further, the disturbance dynamo electric field is slowly varying and associated with the meridional circulation from polar to equatorial latitudes that perturb the low-latitude ionosphere during and up to about a day or two after the onset of geomagnetic storm. The disturbance dynamo electric field is westward in dayside, thus reducing the ambient ionospheric electric field, and eastward in nightside. The storm-induced ionospheric electric field perturbations redistribute the ionospheric plasma and affect the occurrence of plasma density irregularities at equatorial and low latitudes [e.g., *Fejer*, 1986; *Abdu*, 1997; *Sastri et al*., 2000; *Basu et al*., 2005; *Bagiya et al*., 2011].

It is now known that the low-latitude ionospheric electron density varies in response to geomagnetic storm either through electrodynamical and/or neutral-dynamical changes [e.g., *Bagiya et al*., 2009, 2011, and references cited therein]. The magnitude of these variations depends on the intensity and duration of the storm in addition to the season and local time [*Pallamraju et al*., 2004]. Despite significant efforts made in the past several decades to understand the changes in the low-latitude ionosphere during geomagnetic storms, low-latitude ionospheric variabilities corresponding to prolonged geomagnetically disturbed period have not been addressed extensively. This is particularly important as combined and, sometimes, competing effects of electrodynamical/neutral-dynamical and compositional changes determine the ionospheric response over low latitudes when geomagnetic disturbance persists for longer duration. Understanding the role of these individual processes, the hemispherical differences during prolonged geomagnetically disturbed periods is the key element in gauging the response of low-latitude ionosphere in totality. The present exercise is a modest attempt in this direction. In order to address the above mentioned objective, the low-latitude ionospheric electron density variations at various altitudes are derived using ground- and satellite-based observations during 14–17 July 2012 which includes a period of prolonged southward interplanetary magnetic field (IMF B_z). These results are presented and discussed in the subsequent sections. It is expected that the global consequences of such large-duration geomagnetic storms in the ionosphere thermosphere regions presented in this study through observations would be useful not only to appreciate the extent of these effects but also to understand the intricacies of high- to low-latitude interactions during geomagnetic storms.

2. Data Set

The evolution and progress of the geomagnetic storm are represented in terms of variations in basic interplanetary and geomagnetic parameters, i.e., north-south (*Z*) component of interplanetary magnetic field (IMF B_z), auroral electrojet (*AE*) index, and symmetric ring current (*SYM-H*) index. The interplanetary data are obtained from ACE spacecraft measurements at L1 point. In order to examine the effects of interplanetary electric field over the low-latitude ionosphere, the dawn-to-dusk (*Y*) component of IEF (IEF*y*) was derived from IMF B_z and velocity V_x and corrected for the time delay from L1 to the Earth's ionosphere [*Chakrabarty et al*., 2005].

The Global Positioning System (GPS)-total electron content (TEC), altitudinal profile of electron density measured via COSMIC Radio occultation experiment, and Digisonde Portable Sounder (DPS-4D) ionosonde f_oF_2 serve as the basic data of the ionosphere in the present study. TEC observations from GAGAN (GPS aided geo augmented navigation), the Indian SBAS, GPS network chain at Trivandrum (8.49°N, 76.9°E; magnetic latitude 0.18°S), Hyderabad (17.45°N, 78.47°E; magnetic latitude 8.58°N), Bhopal (BPL) (23.28°N, 77.34°E; magnetic latitude 14.45°N), Kolkata (KOL) (22.64°N, 88.44°E; magnetic latitude 13.05°N), and individual low-latitude stations, namely, Ahmedabad (AMD) (23.02°N, 72.51°E; magnetic latitude 14.63°N) and Dibrugarh (DBR) (27.30°N, 94.6°E; magnetic latitude 19.04°N), are considered to investigate the response of low and equatorial ionosphere during the storm. TEC observations from one of the IGS stations, Diego Garcia (DGR) (7.27°S, 72.37°E; magnetic latitude 15.53°S), which is magnetically conjugate to AMD, are presented to investigate the hemispherical differences in the TEC variations, if any. The procedure to estimate the TEC and removal of biases for GAGAN stations is explained in *Rajat et al*. [2007]. Similar method is followed to derive the TEC for Ahmedabad and Dibrugarh. The procedure for TEC derivation from IGS data can be found in *Laskar et al*. [2013]. The elevation mask of 30° is used here to minimize the multipath effects in TEC. In addition to TEC, altitudinal variations of electron density derived from different COSMIC satellites using GPS occultation measurements are extracted for the latitude span of 40°N to 40°S and longitude span of 65°E to 105°E to investigate the altitudinal variations of electron density during the different phases of the storm. The six low Earth-orbiting satellites of COSMIC constellation fly at an altitude of ~800 km with an inclination of ~72°. With the advent of Global Navigation Satellite Systems (GNSS) satellites, radio occultation has emerged as a powerful technique to sound the atmosphere-ionosphere vertically with high resolution and accuracy. In this technique, the low Earth-orbiting satellites receive the signals transmitted by the GNSS satellites. The GNSS signals get refracted due to the ionized medium in their way from GNSS to low Earth-orbiting satellites giving information on the state of the medium almost instantaneously. The change in the relative positions between GNSS and low Earth-orbiting satellites provides an opportunity to scan the intermediate medium vertically. Further technical details on this can be found elsewhere [e.g., *Komjathy et al*., 2010].

One of the shortcomings of the COSMIC RO measurements is its poor temporal coverage over a specific location. In spite of this, the available electron density profiles during different times of the day during different satellite passes over the above mentioned latitude-longitude span have been derived and plotted here. Apart from satellite-based observations, the height-integrated electron density, i.e., TEC, and the in situ observations, i.e., COSMIC electron density profiles, the available DPS f_oF_2 measurements from Ahmedabad are also examined to delineate the storm effects at ionospheric peak altitudes at different times of the day.

The storm time neutral composition variability has pronounced effects on low-latitude ionospheric electron density. In the present case, an attempt is made to explore the thermospheric neutral composition changes due to the excess energy deposition at high latitudes for an extended period and their implications for the low-latitude ionosphere. To realize this goal, the [O/N_2] observations from TIMED/GUVI satellite are extracted and global maps of the same are reproduced here. The TIMED satellite flies in a circular polar orbit at an altitude of 630 km and with an inclination of 74.1°. The Global Ultraviolet Imager (GUVI) instrument on board the TIMED satellite records far ultraviolet (fuv) emissions from photoelectron impact excitation of molecular nitrogen (N_2) and atomic oxygen (O) in the lower and upper thermospheric altitude range of ~130 to ~400 km and derives columnar O/N_2 ratio [*Christensen et al*., 2003]. It is known that N_2 fuv band emission peaks at ~ 150 km while the fuv emission from O is observed at *F* region peak also. Thus, the direct correlation of *F* region electron density with O/N_2 ratio does have some ambiguity, but it is also accepted that in the absence of any other clear measurements, the GUVI-provided O/N_2 ratio can be taken as an indicator of

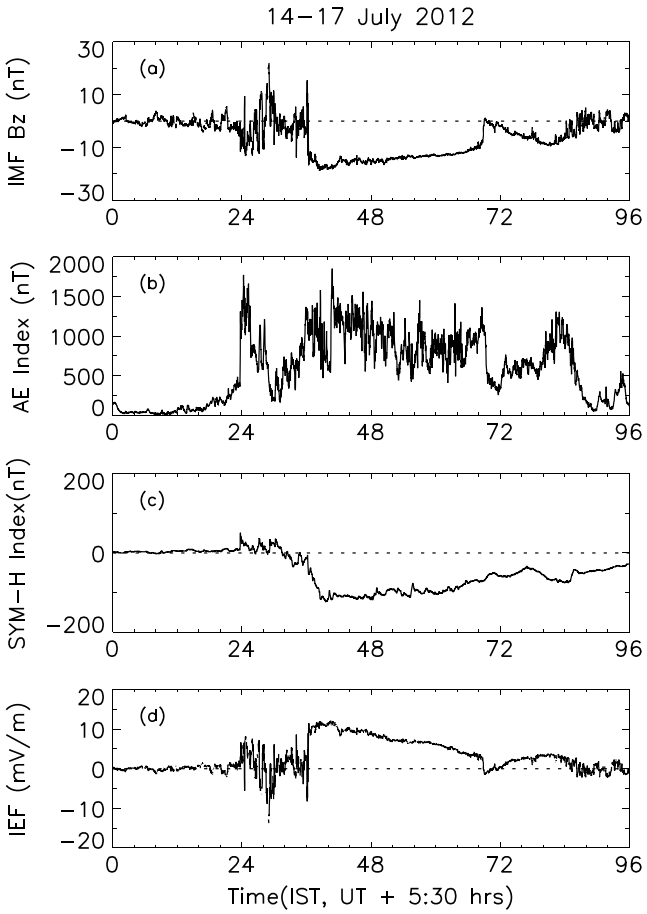

Figure 1. From top, (a) the variations of north-south component of interplanetary magnetic field (IMF) B_z, (b) auroral electrojet (*AE*) index, (c) symmetric ring current (*SYM-H*) index, and (d) dawn-to-dusk component of interplanetary electric field (IEF*y*) during 14–17 July 2012. The IMF B_z turned southward at 12:21 IST on 15 July and continued to be southward till 21:01 IST on 16 July that amounted to a total southward duration of ~33 h. The *AE* index variations illustrated the consistent energy deposition for the similar period of time. A moderate but prolonged geomagnetic storm was observed in *SYM-H* index. The IEF*y* had enhanced at the time of starting of reduction in *SYM-H* and retained the consistent positive values during an extended period of more than 30 h.

thermospheric neutral compositional changes at higher altitudes also. The details of the (GUVI) instrument, operation, and example of data products are presented by *Paxton et al*. [1999] and *Christensen et al*. [2003].

The storm time high-latitude electric field and wind-induced disturbance dynamo electric field alter the equatorial electrojet (EEJ) current, the former promptly and the latter after a time delay. The EEJ strength ($\Delta H_{(TIRUNELVELI)} - \Delta H_{(ALIBAG)}$) is derived from the ground perturbations of the horizontal component of the geomagnetic field (ΔH) values at Alibag (18.46°N, 72.87°E; magnetic latitude 10.19°N) and at Tirunelveli (8.70°N, 77.80°E; magnetic latitude 0.03°N) during the storm period as per the method adopted by *Rastogi and Klobuchar* [1990]. In the ensuing part of this work, TEC refers to vertical TEC. The time format everywhere is Indian Standard Time (IST), except TIMED/GUVI observations wherein time is in UT.

3. Results

An eruption of an earthward CME along with X1.4 class solar flare from sunspot AR1520 had occurred at 23:26 IST (16:53 UT) on 12 July 2012. IMF B_z was observed to turn southward at 21:22 IST (15:52 UT) on 14 July 2012. The variations of various interplanetary and geomagnetic parameters are shown in Figure 1 for the period of 14–17 July 2012. The IMF B_z (Figure 1a) was fluctuating from south to north between 21:22 IST (15:52 UT) on 14 July and 12:20 IST (06:50 UT) on 15 July. Intensification of *AE* with the southward turning of IMF B_z is also noticed (Figure 1b). The storm sudden commencement (SSC) had occurred at 23:44 IST (18:14 UT) on 14 July 2012 as observed in *SYM-H* Index (Figure 1c). The sharp reduction in *SYM-H* at 10:49 IST (05:19 UT) on 15 July marked the beginning of the storm main phase. The variation of IEF*y* is shown in Figure 1d. At 12:21 IST (06:51 UT) on 15 July, IMF B_z abruptly turned southward and retained the direction till 21:02 IST (15:30 UT) on 16 July (~33 h). A sharp reduction in *SYM-H* also occurred in simultaneity on 15 July resulting in a moderate geomagnetic storm with *SYM-H* minimum value of −123 nT at 15:35 IST (10:05 UT). The IEF*y* had reached to ~11 mV/m at the time of starting of reduction in *SYM-H* and retained the consistent positive values during an extended period of more than 30 h. A very slow recovery was seen in *SYM-H* after 00:00 IST (18:30 UT on 15 April) on 16 April with very gradual decrease in the IMF B_z. After approaching the recovery for the active period of ~33 h, IMF B_z turned southward again on 16 July at 21:27 IST (15:57 UT). The weak geomagnetic activity was again seen in IMF B_z, *AE*, *SYM-H*, and in IEF*y* on 16 and 17 July.

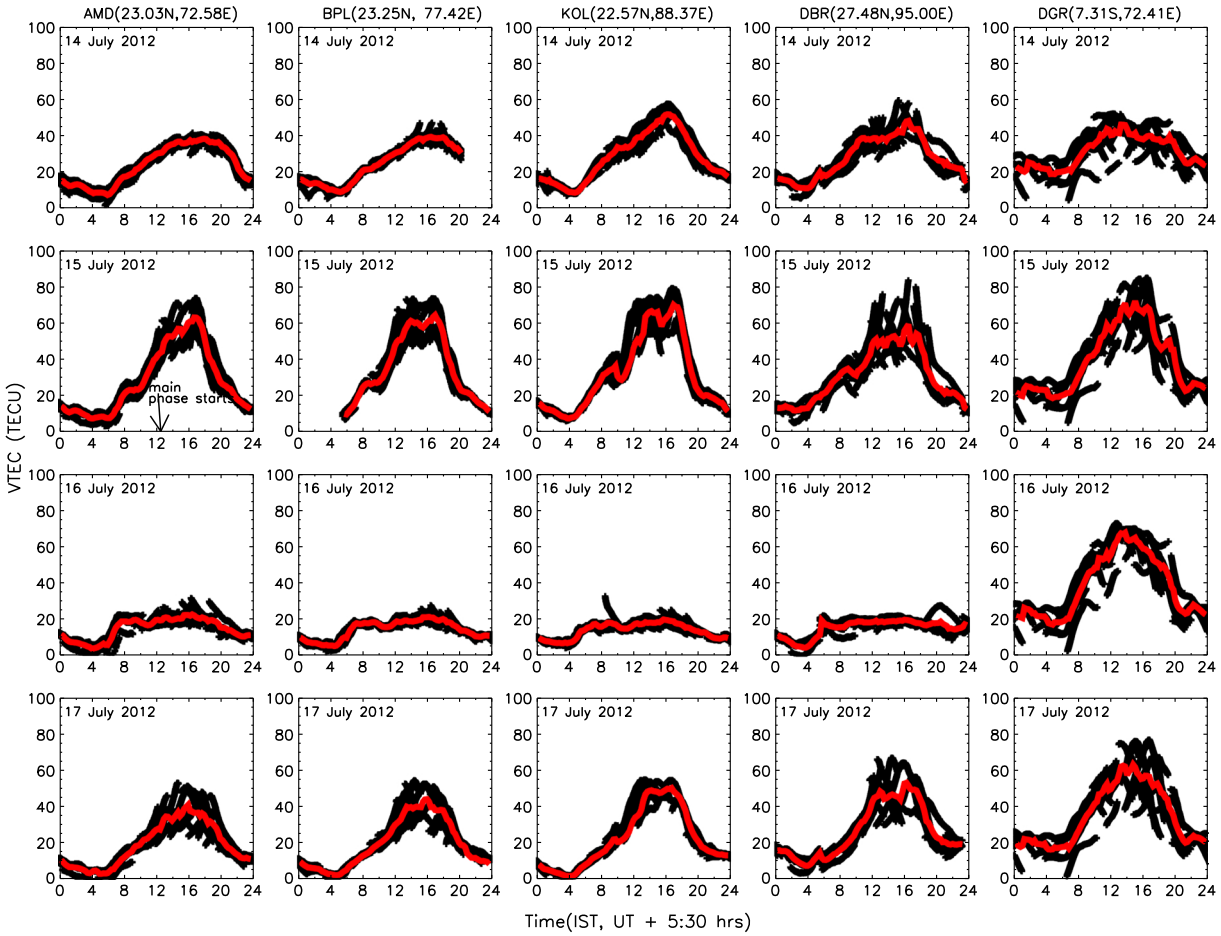

Figure 2. Low-latitude TEC variations in the Northern Hemispheric stations (first column) AMD (14.45°N, magnetic latitude), (second column) BPL (13.05°N, magnetic latitude), (third column) KOL (14.63°N, magnetic latitude), (fourth column) DBR (19.04°N, magnetic latitude) are shown and in the Southern Hemispheric station (fifth column) DGR (15.53°S, magnetic latitude), during 14–17 July 2012. DGR is magnetically conjugate to AMD. The low-latitude TEC values were enhanced in both hemispheres on 15 July showing the positive ionospheric storm effect. However, on 16 July, a strong negative ionospheric storm was observed over the northern hemispheric low latitudes while at the Southern Hemisphere, TEC values were higher compared to the geomagnetically quiet day. The reduction in the peak TEC values at northern hemispheric stations were greater than 60% compared to the corresponding peak values on the quiet day. The TEC values recovered to normal day values on 17 July.

Figures 2–5 depict the low-latitude ionospheric behavior during the storm period of 14–17 July. In Figure 2, the first four columns represent TEC variations at northern hemispheric low-latitude stations AMD, BPL, KOL, and DBR. The TEC observations in the figure are put in the ascending order of longitude. The rightmost (fifth) panel shows the TEC variations over southern hemispheric low-latitude station DGR. The black lines in each plot indicate TEC from different satellites passing over the respective station during the course of the day. The red line shows the mean TEC values at every 15 min from all visible satellites in the field of receiver at that epoch. Figure 2 (top row) plotted for 14 July can be considered as the geomagnetic quiet day diurnal TEC variations. The characteristic peak, delayed in time, was observed at all stations as they are located either near equatorial ionization anomaly (EIA) crest or beyond EIA crest region. The mean peak TEC values were between 40 and 50 total electron content unit, 1 TECU = 10^{16} el m^{-2} (TECU) at both the hemispheric stations on 14 July. A clear longitudinal TEC variability was seen at northern low latitudes with larger more TEC magnitudes over KOL and DBR and smaller over AMD and BPL. The TEC over the magnetically conjugate stations, AMD and DGR, show clear seasonal dependence, with ~9 TECU larger magnitudes over DGR than AMD. This aspect will be discussed in detail later in the text. Figure 2 (second row) shows the response of low-latitude TEC on the storm commencement day of 15 July. The time of abrupt southward turning of IMF B_z and corresponding reduction in *SYM-H* is shown by an arrow in the first plot of the panel. The diurnal mean TEC peak was enhanced to ~63, 64, 70, 60, and 72 TECU over AMD, BPL, KOL, DIB, and DGR, respectively.

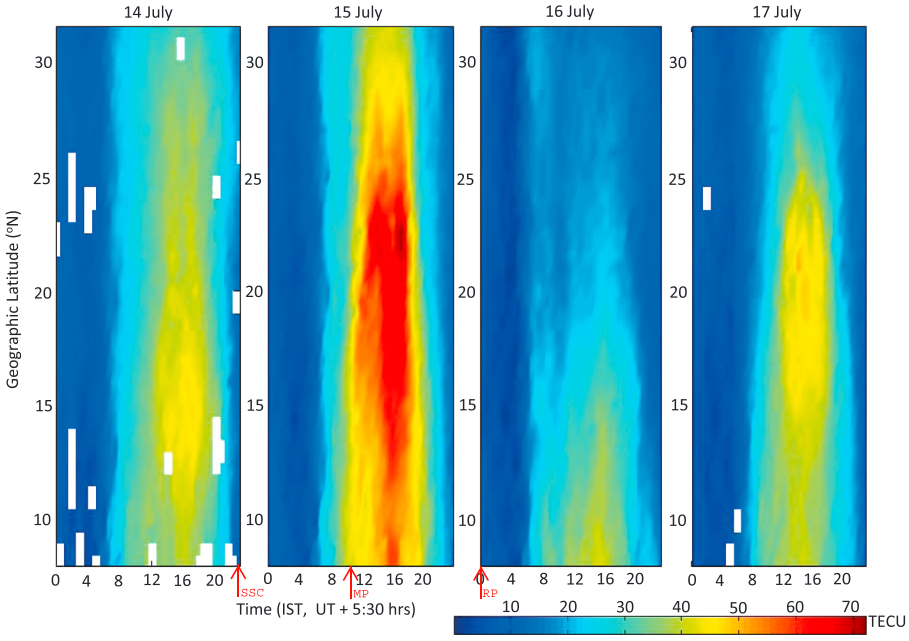

Figure 3. Latitudinal and temporal variations of TEC showing the development of equatorial ionization anomaly (EIA) in the Northern Hemisphere during 14–17 July 2012. The sudden storm commencement (SSC), main phase (MP) onset, and the starting of recovery phase (RP) are shown in the figure. TEC was enhanced over larger latitudinal belt starting from the magnetic equator to the northern crest of EIA on 15 July. On 16 July, EIA peak was completely absent and developed normally on the following day.

The enhancements of ~20 TECU in diurnal mean TEC with respect to quiet day indicate the positive ionospheric storm effects over low latitudes on 15 July. Figure 2 (third row) depicts the low-latitude diurnal TEC variations along with the mean TEC on 16 July. It could be seen that an unusual strong reduction in TEC was observed on most of the daytime hours. The TEC over AMD, BPL, KOL, and DBR reached their quiet day's nighttime values during the day. The decrease in TEC was ~40 to 50 TECU (60%–72%) in comparison to previous day's TEC and ~15 to 30 TECU (40%–62%) in comparison to a typical quiet day's TEC. The observed deep TEC reduction indicated the absence of most of the daytime electron density at low latitudes in the Northern Hemisphere. On the contrary, in the Southern Hemisphere, TEC at DGR did not reveal this feature as can be seen in Figure 2 (fifth column). A maximum TEC of ~68 TECU was observed over DGR on 16 July, just 4 TECU lesser than 15 July but ~26 TECU higher than quiet day's TEC. Figure 2 (bottom row) reveals that on 17 July, the diurnal TEC recovered to normal values. The TEC variations stated above pertain to near EIA or beyond EIA crest region. It is interesting to note that the TEC values over DGR do not show such drastic variations as seen in the Northern Hemisphere.

In order to study the storm time TEC variations over larger latitudinal belt, the latitudinal plots of TEC at different times of day using GAGAN GPS network are prepared and shown in Figure 3. The figure shows EIA development along 77°E longitude during 14–17 July. On 14 July, the northern flank of EIA was rather moderately developed. The peak occurred at ~16° geographic north. The second plot shows the EIA behavior on 15 July. It could be noted that strong EIA had developed on 15 July, with TEC enhancements from the equator to the northern EIA crest. The third plot of Figure 3 shows that EIA was completely suppressed on 16 July and its peak was not seen at all. As mentioned earlier, it is interesting to observe that TEC beyond 20° geographic north reached its quiet time nightly values during daytime. On 17 July, EIA recovered to normal values and peak occurred at ~22° geographic north, with large TEC values than those of the quiet day.

Figure 4 represents the altitudinal variations of electron densities at different times of the day derived from COSMIC RO measurements for one of the quiet days, 11 July (black), 15 (blue), and 16 (red) July 2012. The quiet day is selected on the basis of the availability of sufficient number of passes for a given time period in a given hemisphere. As indicated, Figure 4a shows the vertical electron density variations for 0° to 40°N latitude belts while Figure 4b shows for 0° to 40°S. The longitudinal span as mentioned in the figure is restricted to

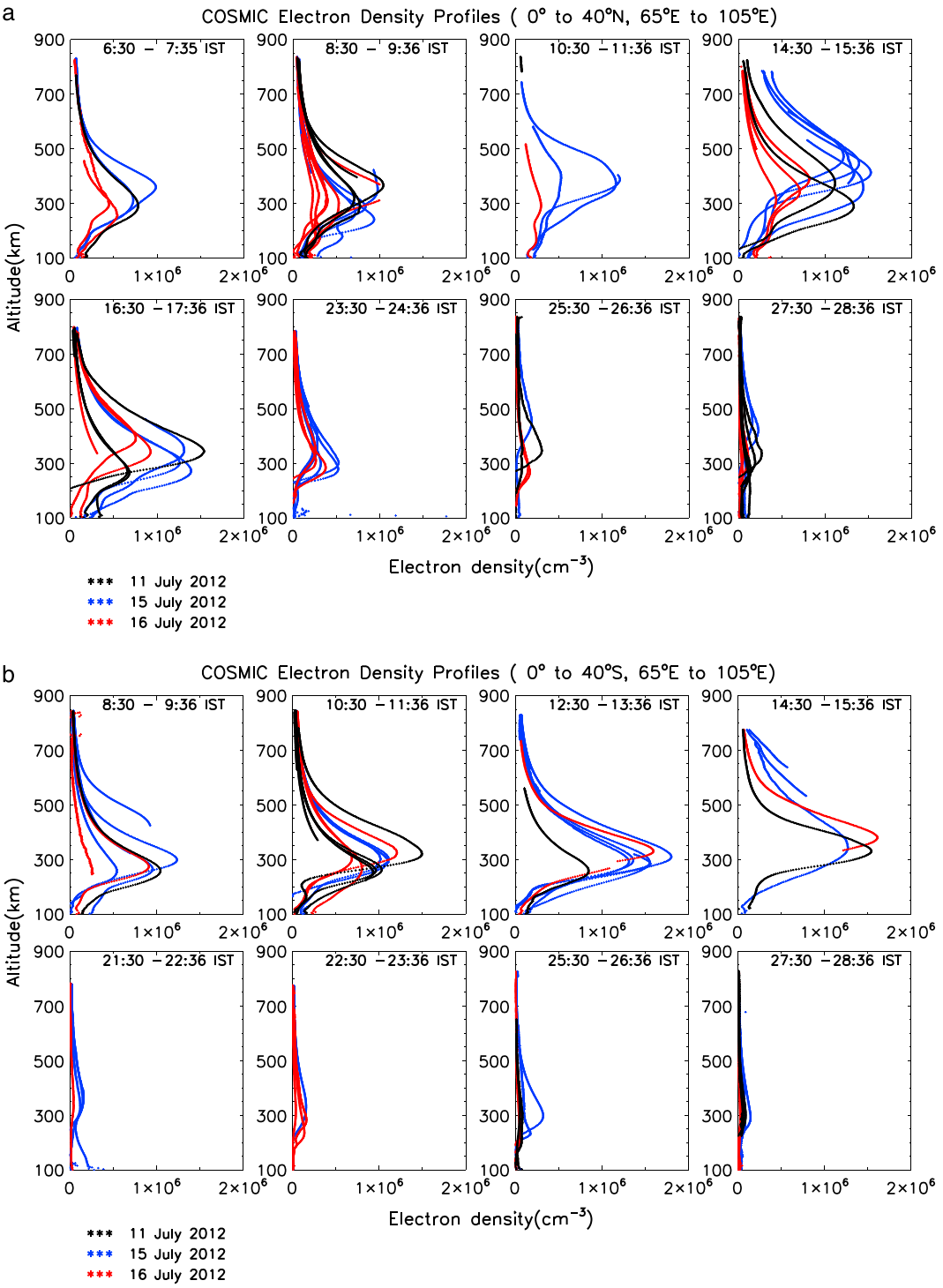

Figure 4. COSMIC RO electron density profiles obtained for different times of the day for 11 (black), 15 (blue), and 16 (red lines) July 2012, (a) for 0° to 40°N and 65° to 105°E geographical region and (b) for 0° to 40°S and 65°E to 105°E geographical region. The broadening of electron density profiles in Figure 4a during 14:30 and 15:35 IST coincides with the time of prompt penetration electric field on 15 July. On 16 July, the ionospheric density profiles were completely suppressed on most of the hours in the daytime in the Northern Hemisphere. The electron density variations in the Southern Hemisphere (Figure 4b) did not show any significant variations except for high-density values during 14:30 to 15:35 IST on 16 July.

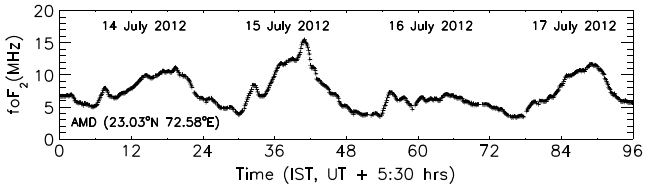

Figure 5. Digisonde-derived f_oF_2 values during 14 to 17 July 2012 obtained from a low-latitude station, Ahmedabad (23.02°N, 72.51°E; magnetic latitude 14.63°N), is shown, which supports the noticeable enhancements and the large reduction in low-latitude maximum ionospheric electron density on 15 and 16 July 2012, respectively.

65°E to 105°E for both the latitudinal regions in order to overlap with the data of Indian longitudes presented in earlier figures. It could be seen that in the Northern Hemisphere, the electron density shows noticeable enhancements over all the altitudes on 15 July between 10:30 and 11:35 IST and 14:30 to 15:35 IST. It is readily seen that the peak in electron density enhancements are more than 15% with respect to quiet day's values between 14:30 to 15:35 IST. It may be noted that this time coincides with the time of strong EIA development (as seen in Figure 3). The electron density on 16 July is observed to be reduced during most of the day with respect to geomagnetic quiet day's values. The maximum reduction in peak electron density is again between 14:30 and 15:35 IST which is of the order of 60% with respect to quiet day. On the other hand, the electron density profiles in the Southern Hemisphere show similar behavior on all the 3 days including those of the quiet day (11 July). It may be noted that on 16 July, the peak electron density between 14:30 and 15:35 IST is greater than the respective peak value on 15 July, in contrast to those of Northern Hemisphere wherein the electron density on the 16 showed smaller values than those on the 15 July.

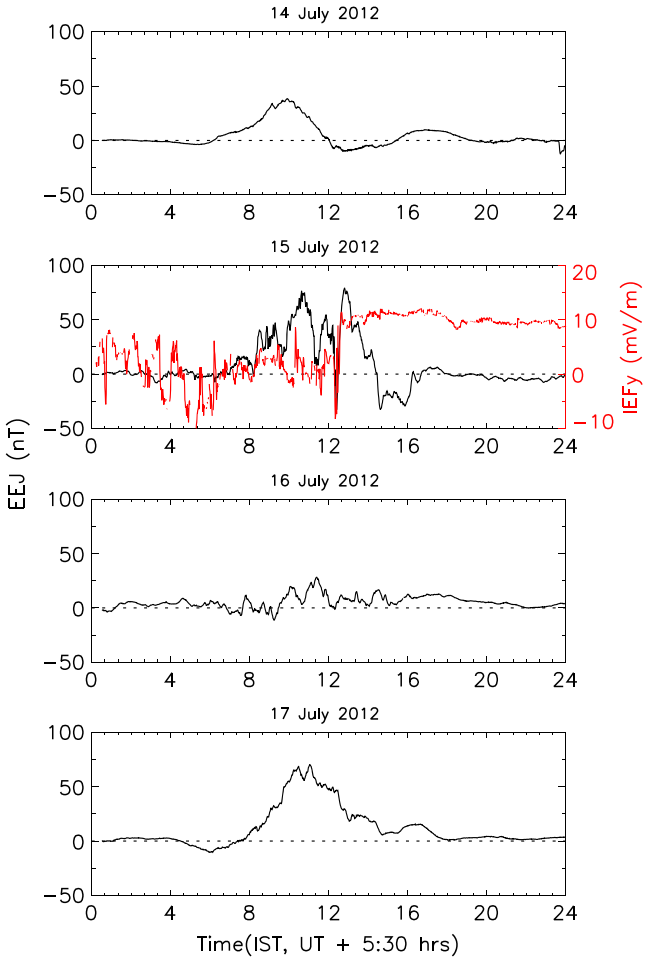

Figure 6. Equatorial electrojet (EEJ) variations during 14–17 July 2012. The dawn-to-dusk component of the IEF*y* is plotted along with the EEJ for 15 July. It can be seen that EEJ strength variations during 1000–1300 IST on 15 July corresponded to the variations in the IEF*y* component. EEJ was completely suppressed during daytime on 16 July and recovered to normal day values on 17 July.

In addition to satellite-based observations, the response of ground-based observations of electron density variations have also been examined during the storm days. Figure 5 represents the Digisonde-derived f_oF_2 measurements (which are related to electron density as $(f_oF_2)^2 \propto N_{max}$) from AMD during 14–17 July 2012. The f_oF_2 shows the presence of positive ionospheric storm with an increase of ~5 MHz at ~17 IST on 15 July 2012 which also coincides with the time of development in the peak EIA in Figure 3. The f_oF_2 on 16 July shows a significant decrease with reduction greater than 35% and 55% in its values as compared to quiet day and 15 July, respectively. It could be seen that after the initial usual buildup in the morning, the f_oF_2 had retained its nighttime values during most of the hours in the daytime. Thus, the high temporal resolution observations from COSMIC and Digisonde (AMD) confirm the GPS-TEC observations and indicate that the electron densities at different

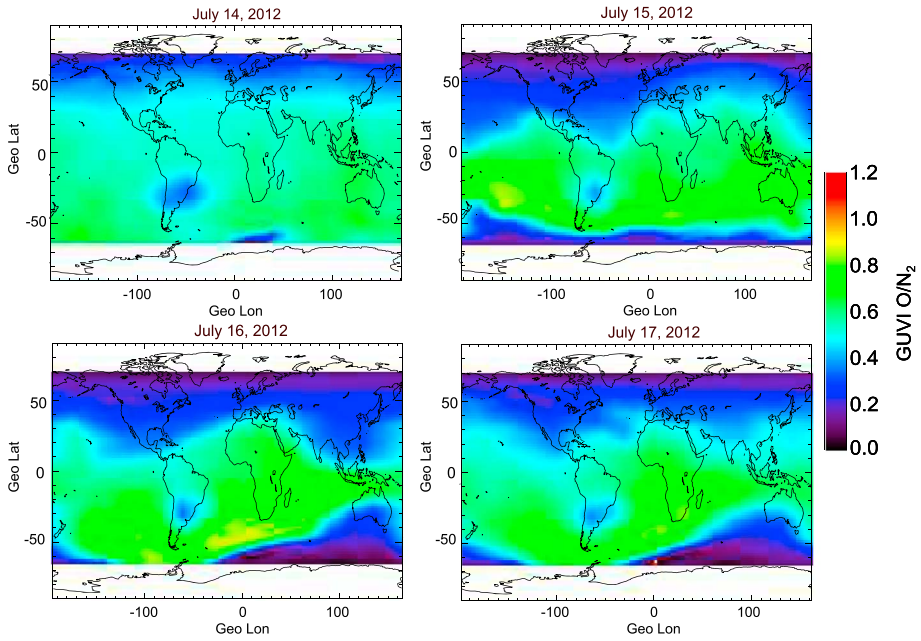

Figure 7. TIMED/GUVI maps of [O/N_2] during 14–17 July 2012. Thermospheric neutral compositional variations in terms of [O/N_2] showed enhancements in atomic oxygen over low latitudes on 15 July while strong depletion in [O/N_2] on 16 July supports the enhancement of molecular nitrogen mainly over the Northern Hemispheric low latitudes. Gradual recovery was observed in [O/N_2] on 17 July.

ionospheric altitudes throughout the low-latitude region responded to the effects of the magnetic disturbance event under consideration.

In order to explore the possible role of storm time electrodynamical and neutral-dynamical processes in generating the observed low-latitude electron density variations, the low-latitude electric field perturbations in terms of equatorial electrojet (EEJ) index and thermospheric neutral composition changes in terms of [O/N_2] variations are analyzed. Figure 6 shows the EEJ variations during 14–17 July. The EEJ developed normally on 14 July with a moderate peak value. Unusual perturbations were observed in EEJ on 15 July with a peak value of ~79 nT at ~12:49 IST. In order to understand this variation, the IEF*y* variations on 15 July were examined and are overplotted on EEJ variations in Figure 6 (red color). It is interesting to note that the variations in the IEF*y* and EEJ agree well during 10:00 to 13:00 IST on 15 July. The sharp reductions in the EEJ strength during midday hours and the possible presence of counter-electrojet in the afternoon hours indicate reduction in time-integrated EEJ strength on 15 July. The development of EIA is directly related to the time-integrated EEJ strength [*Raghavarao et al.*, 1978]. It is interesting to note here that although there was an apparent reduction in the integrated EEJ strength, the northern flank of EIA was well developed on 15 July as shown in Figure 3. This aspect will be discussed in detail in the next section. On 16 July, EEJ was completely suppressed during daytime. The possible role of delayed storm time disturbance dynamo effects in reducing the EEJ strength and the possible implications of storm time interhemispheric winds in transporting the plasma across the equator into the opposite hemisphere is discussed later. The EEJ variation on 17 July shows a normal day pattern indicating the cessation of geomagnetic storm effect on the EEJ.

In order to understand the compositional changes over low latitude during this storm, the thermospheric neutral composition variations have been looked into. Figure 7 shows the TIMED/GUVI map of [O/N_2] ratios. This figure represents the global maps of [O/N_2] variations during 14–17 July. The [O/N_2] variations on 14 July follow normal day behavior with reduced values in the northern (summer hemisphere) polar region. Following the storm event, the enhancement in [O/N_2] was observed globally on 15 July. In the summer hemisphere dayside, the enhancement in [O/N_2] was seen at equatorial and low latitudes while reduction was observed at middle and higher latitudes. This reduction extended up to low and equatorial latitudes in the summer nightside. In the winter hemisphere, the [O/N_2] enhancement was prominently seen at middle to equatorial latitudes. The global [O/N_2] variations were also unusual on 16 July. The strong reduction in [O/N_2]

was observed on most of the Asia Pacific regions. The storm time reduction in $[O/N_2]$ up to equatorial latitudes is rarely seen. On the other hand, $[O/N_2]$ reduction started to recover in the summer nightside. The slow recovery in the $[O/N_2]$ ratio was seen globally on 17 July. The unusual depletion in $[O/N_2]$ up to equatorial latitudes is discussed in terms of global wind variations in the next section.

4. Discussion

In the present exercise, the observed electron density variations could be considered due to both storm time electrodynamical and neutral-dynamical changes over low and equatorial latitudes. The immediate increase in ionospheric electron density following the storm commencement is generally termed as positive ionospheric storm. The occurrence of positive ionospheric storm is, in general, attributed to either the prompt penetration of IEF*y* or enhanced neutral atomic species at respective latitudes depending on the local time and season. As mentioned, the IEF*y* penetration is usually eastward during the day thus enhancing the ambient low-latitude ionospheric electric field. The enhanced ambient electric field raises the *F* region to higher altitudes where recombination effect is less. This results into the enhancement of low-latitude electron density during daytime. The prompt penetration over the equatorial latitudes increases the vertical equatorial E × B drift and thus intensifies the development of EIA. This also ultimately increases the low-latitude electron density in dayside. The physical mechanism of storm time prompt penetration of IEF*y* to low latitudes and its role in positive ionospheric storm are discussed in the literature [e.g., *Pallamraju et al*., 2004; *Tsurutani et al*., 2004; *Lin et al*., 2005; *Zhao et al*., 2005; *Balan et al*., 2010; *Bagiya et al*., 2011 etc.]. The similarities in the fluctuations in IEF*y* and EEJ strength during 10:00–13:00 IST on 15 July suggest prompt penetration of IEF*y* to equatorial latitudes during this time. Nevertheless, as already stated, the integrated EEJ strengths were clearly small on this day. As the distribution of plasma over low latitudes is found to depend significantly on the integrated EEJ strength [*Raghavarao et al*., 1978], the enhancements of TEC throughout the Indian low-latitude region on 15 July cannot be explained by the enhanced fountain effect owing to the effects of IEF*y* on the zonal electric field over equatorial latitudes. However, it is possible that TEC enhancements on this day are partially due to the eastward electric field perturbations throughout the low-latitude region that can take the *F* region plasma to higher altitudes where recombination is less. This aspect is readily observed in the vertical electron density profile between 14:30 and 15:35 IST in Figures 4a and 4b. It could be seen that the whole ionosphere is lifted to higher altitudes during this time period. It should also be noticed that the ionosphere has taken a finite time to respond to the abrupt enhancements in IEF*y*. Due to the less number of satellite passes, only one satellite showing the upliftment between 14:30 and 15:35 IST could be obtained in the Southern Hemisphere. But the broader layer thickness of the ionosphere during this time period is clearly seen on this day (15 July) as compared to other days in this observation. Using a combination of GPS-TEC and f_oF_2 observations from the chain of ionosondes distributed along a meridian of 280°E in South America, *Zhao et al*. [2012] have carried out a case study on the contribution of topside and bottomside ionospheres to the positive ionospheric storm observed over this longitude during the super storm of 20 November 2003. It would be interesting to investigate separately the topside and bottomside ionospheric response to the addressed prolonged geomagnetic storm event.

In addition to the prompt penetration effect, it is also evident from the global $[O/N_2]$ map that atomic oxygen might have increased over low latitudes on 15 July. Atomic oxygen (O) is directly responsible for the production of plasma at *F* region heights. Thus, enhanced O and vertical movement of *F* region over low latitudes contribute to the observed electron density enhancements in the Northern Hemisphere, particularly around the northern EIA crest region as observed in TEC as well as in f_oF_2 on 15 July. The strong negative ionospheric storm on 16 July over the Indian low-latitude stations in the Northern Hemisphere could have been assisted by various factors. During northern summer (July), the negative ionospheric storm effects would be more enhanced due to the increase in the supply of vibrationally excited N_2 from the high-latitude region leading to more recombination of available local plasma [*Prölss and Werner*, 2002]. However, reduction of TEC by more than 60% with respect to quiet day TEC is quite significant. *Sastri* [1988] had reported the geomagnetic storm time ionospheric electron density reduction (of the order of ~ 15%) in the Northern Hemisphere during summer and equinoxes using ionosonde observations in the 72°–85°E longitude sector. Independent case studies [e.g., *Lynn et al*., 2004; *Liou et al*., 2005] had also brought out negative ionospheric storm characteristics over low latitudes. But the electron density reduction observed in the present case is very large compared to that reported in other studies. *Wang et al*. [2013] had studied the ionospheric

variability over North China during 15–16 July 2012 storm using multiinstrumental observations. No attempt was made by them to bring out the clear roles of the possible physical mechanisms responsible behind the observed ionospheric variability over the midlatitude stations of North China during this prolonged geomagnetic storm event.

The delayed ionospheric electric field perturbations due to storm time disturbance dynamo effects, westward during daytime, can cause EEJ to be weakened and can lead to weakly developed EIA. The suppressed EEJ current on 16 July indicates the effects of delayed disturbance dynamo at low and equatorial latitudes. As a consequence, the development of EIA can be expected to be weak and this is apparent from the complete absence of the northern EIA crest in TEC as well as in f_oF_2 from AMD. Interestingly, EIA crest region in the Southern Hemispheric station (DGR) shows significant increase in TEC in contrast to the substantial decreases in the northern hemispheric stations. The electron density profiles also revealed that in the Southern Hemisphere, the electron density values do not vary much between the quiet day and geomagnetic storm day of 15 July. The asymmetry in TEC at conjugate EIA crest regions, AMD and DGR as well as the difference in satellite-based electron density observations in both hemispheres, indicate the possible role of winds in distribution of ionization over low latitudes. It is known that the continuous energy deposition at high latitudes during the prolonged southward IMF B_z conditions produces the heating of polar ionosphere, which sets up strong pole to equator meridional winds in both hemispheres. The strong equatorward disturbance winds are in phase with the summer to winter interhemispheric winds in the Northern (summer) Hemisphere and of opposite phase in the Southern (winter) Hemisphere. This enhanced wind system coupled with the daytime poleward wind is believed to have transported the plasma significantly across the equator into the Southern Hemisphere as can be seen by the strong southern EIA crest in spite of a very weak EEJ on 16 July. Though the role of winds is clearly visible here in transporting the ionization to the southern winter hemisphere, the observed strong reduction in $[O/N_2]$ at low latitudes in summer hemisphere must have also played a major role in creating the strong TEC reduction at low latitudes. The depletion in $[O/N_2]$ may be either due to reduction in atomic oxygen or enhancement in N_2 or both. The storm time depletion in $[O/N_2]$ is more effectively seen in summer nightside where all winds, i.e., meridional, seasonal, and diurnal get superimposed. Therefore, the molecular rich air (reduced $[O/N_2]$) reaches first at summer nightside and moves farther toward low latitudes and gets transported to the dayside with the rotation of the Earth. It is interesting to note the strong and extended $[O/N_2]$ reduction in the western longitudes (which were in nightside when geomagnetic disturbances started) on 15 July. It seems that the molecular rich air had traveled to the eastern longitudes on 16 July from the nightside. The combined effects of the transport with the rotation of the Earth and the direct transport from high latitudes had produced the strong $[O/N_2]$ depletion which extended up to low and equatorial latitudes on 16 July. Such significant molecular enhancements at low latitudes over Indian region could be responsible for the strong negative ionospheric storm on 16 July. Strong TEC depletions of 16 July had recovered to the normal level on 17 July. It could also be seen that TEC was little higher on 17 July compared to the quiet days TEC and EIA also developed comparatively strongly. The low-latitude TEC increase on 17 July could be due to the high strength of EEJ.

This paper, thus, presents observational evidence of the large-scale (both in time and space) effects of a long duration geomagnetic storm using a suite of ground-based and satellite-borne data sets, right from the initiation to the recovery of the geomagnetic storm. This brings to light the asymmetric response with respect to latitudes in the ionospheric-thermospheric constituents over low and middle latitudes that seem to exist during the geomagnetic storms that occur during solstices.

5. Summary

The present case study captures the significant changes in the ionospheric electron density and thermospheric neutral composition during the prolonged southward IMF B_z condition that prevailed during 15–16 July 2012. Drastic changes in the electron density throughout the low-latitude region are observed during this event. During the early phase of the southward IMF B_z condition (15 July 2012), the effects of positive ionospheric storm seem to dominate over the plasma fountain effect (essentially driven by the zonal *E* region electric field). This explains the enhanced TEC over the low-latitude region despite integrated EEJ strength being small. In addition, large electron density reduction on 16 July is observed as a consequence of modification of the effects of negative ionospheric storm by neutral compositional disturbances and various

wind systems. This resulted in a decrease in TEC throughout the northern low-latitude stations and its increase in the Southern Hemispheric station. Therefore, corresponding to longer duration of the southward IMF B_z condition, the combined effects of positive/negative ionospheric storms, equatorial electrodynamics, and wind systems will determine the eventual ionospheric electron density over low latitudes.

Acknowledgments

The GAGAN GPS data are part of the GAGAN project, a joint collaboration between ISRO and Airports Authority of India. The RINEX format GPS observational and navigational data are obtained from the International GNSS Service (IGS) network. The authors duly acknowledge the TACC and CDACC team members for providing the COSMIC data. The authors thank NASA/GSFC CDAWeb team for the interplanetary data, WDC-C2 (Kyoto) for the auroral electrojet and geomagnetic indices data, and NASA and MO&DA program for the GUVI data. The work of F.L., D.C., and D.P. is supported by the Department of Space, Government of India. R.H. is thankful to the CSSTEAP (Centre for Space Science and Technology Education in Asia and Pacific) for giving the opportunity to work in a pilot project at PRL. TEC data for DBR were obtained as part of the ISRO SSPS initiative. The authors thank the editor and the reviewers for their constructive comments.

Alan Rodger thanks George Millward and an anonymous reviewer for their assistance in evaluating this paper.

References

Abdu, M. A. (1997), Major phenomena of the equatorial ionosphere-thermosphere system under disturbed conditions, *J. Atmos. Sol. Terr. Phys.*, *59*, 1505–1519.

Bagiya, M. S., H. P. Joshi, K. N. Iyer, M. Aggarwal, S. Ravindran, and B. M. Pathan (2009), TEC variations during low solar activity period (2005–2007) near the equatorial ionospheric anomaly crest region in India, *Ann. Geophys.*, *27*, 1047–1057.

Bagiya, M. S., K. N. Iyer, H. P. Joshi, S. V. Thampi, T. Tsugawa, S. Ravindran, R. Sridharan, and B. M. Pathan (2011), Low-latitude ionospheric-thermospheric response to storm time electrodynamical coupling between high and low latitudes, *J. Geophys. Res.*, *116*, A01303, doi:10.1029/2010JA015845.

Balan, N., K. Shiokawa, Y. Otsuka, T. Kikuchi, D. Vijaya Lekshmi, S. Kawamura, M. Yamamoto, and G. J. Bailey (2010), A physical mechanism of positive ionospheric storms at low latitudes and midlatitudes, *J. Geophys. Res.*, *115*, A02304, doi:10.1029/2009JA014515.

Basu, S., et al. (2005), Two components of ionospheric plasma structuring at midlatitudes observed during the large magnetic storm of October 30, 2003, *Geophys. Res. Lett.*, *32*, L12S06, doi:10.1029/2004GL021669.

Blanc, M., and A. D. Richmond (1980), The ionospheric disturbance dynamo, *J. Geophys. Res.*, *85*, 1669–1686, doi:10.1029/JA085iA04p01669.

Burns, A. G., T. L. Killeen, and R. G. Roble (1991), A theoretical study of thermospheric composition perturbations during an impulsive geomagnetic storm, *J. Geophys. Res.*, *96*, 14,153–14,167, doi:10.1029/91JA00678.

Burns, A. G., T. L. Killeen, W. Deng, G. R. Carignan, and R. G. Roble (1995), Geomagnetic storm effects in the low- to middle-latitude upper thermosphere, *J. Geophys. Res.*, *100*, 14,673–14,691, doi:10.1029/94JA03232.

Chakrabarty, D., R. Sekar, R. Narayanan, C. V. Devasia, and B. M. Pathan (2005), Evidence for interplanetary electric field effect on the OI 630.0 nm airglow over low latitudes, *J. Geophys. Res.*, *110*, A11301, doi:10.1029/2005JA011221.

Chakrabarty, D., R. Sekar, R. Narayanan, A. K. Patra, and C. V. Devasia (2006), Effects of interplanetary electric field on the development of an equatorial spread-F event, *J. Geophys. Res.*, *111*, A12316, doi:10.1029/2006JA011884.

Christensen, A. B., et al. (2003), Initial observations with the Global Ultraviolet Imager (GUVI) in the NASA TIMED satellite mission, *J. Geophys. Res.*, *108*(A12), 1451, doi:10.1029/2003JA009918.

Crowley, G., et al. (2006), Global thermosphere-ionosphere response to onset of 20 November 2003 magnetic storm, *J. Geophys. Res.*, *111*, A10S18, doi:10.1029/2005JA011518.

Fejer, B. G. (1986), Equatorial ionospheric electric fields associated with magnetospheric disturbances, in *Solar Wind Magnetosphere Coupling*, edited by Y. Kamide and J. A. Slavin, pp. 519–545, Terra Sci, Tokyo, Japan.

Fuller-Rowell, T. J., M. V. Codrescu, R. J. Moffett, and S. Quegan (1996), On the seasonal response of the thermosphere and ionosphere to geomagnetic storms, *J. Geophys. Res.*, *101*, 2343–2353, doi:10.1029/95JA01614.

Fuller-Rowell, T. J., M. V. Codrescu, R. G. Roble, and A. D. Richmond (1998), How does the thermosphere and ionosphere react to a geomagnetic storm?, in *Magnetic Storms*, *Geophys. Monogr. Ser.*, vol. 98, edited by B. T. Tsurutani et al., pp. 203–225, AGU, Washington, D. C.

Immel, T. J., G. Crowley, J. D. Craven, and R. G. Roble (2001), Dayside enhancements of thermospheric O/N_2 following magnetic storm onset, *J. Geophys. Res.*, *106*(A8), 15,471–15,488, doi:10.1029/2000JA000096.

Komjathy, A., B. Wilson, X. Pi, V. Akopian, M. Dumett, B. Iijima, O. Verkhoglyadova, and A. J. Mannucci1 (2010), JPL/USC GAIM: On the impact of using COSMIC and ground-based GPS measurements to estimate ionospheric parameters, *J. Geophys. Res.*, *115*, A02307, doi:10.1029/2009JA014420.

Kozyra, J. U., V. K. Jordanova, J. E. Borovsky, M. F. Thomsen, D. J. Knipp, D. S. Evans, D. J. McComas, and T. E. Cayton (1998), Effects of a high-density plasma sheet on ring current development during the November 2–6, 1993, magnetic storm, *J. Geophys. Res.*, *103*, 26,285–26,306, doi:10.1029/98JA01964.

Laskar, F. I., D. Pallamraju, T. V. Lakshmi, M. A. Reddy, B. M. Pathan, and S. Chakrabarti (2013), Investigations on vertical coupling of atmospheric regions using combined multiwavelength optical dayglow, magnetic, and radio measurements, *J. Geophys. Res. Space Physics*, *118*, 4618–4627, doi:10.1002/jgra.50426.

Lin, C. H., A. D. Richmond, J. Y. Liu, H. C. Yeh, L. J. Paxton, G. Lu, H. F. Tsai, and S.-. Y. Su (2005), Large-scale variations of the low-latitude ionosphere during the October–November 2003 superstorm: Observational results, *J. Geophys. Res.*, *110*, A09S28, doi:10.1029/2004JA010900.

Liou, K., P. T. Newell, B. J. Anderson, L. Zanetti, and C.-I. Meng (2005), Neutral composition effects on ionospheric storms at middle and low latitudes, *J. Geophys. Res.*, *110*, A05309, doi:10.1029/2004JA010840.

Lu, G., X. Pi, A. D. Richmond, and R. G. Roble (1998), Variations of total electron content during geomagnetic disturbances, *Geophys. Res. Lett.*, *25*, 253–256, doi:10.1029/97GL03778.

Lynn, K. J. W., M. Sjarifudin, T. J. Harris, and M. Le Huy (2004), Combined TOPEX/Poseidon TEC and ionosonde observations of negative low-latitude ionospheric storms, *Ann. Geophys.*, *22*, 2837–2847.

Mac-Mahon, R. M., and W. D. Gonzalez (1997), Energetics during the main phase of geomagnetic superstorms, *J. Geophys. Res.*, *102*, 14,199–14,207, doi:10.1029/97JA01151.

Pallamraju, D., S. Chakrabarti, and C. E. Valladares (2004), Magnetic storm-induced enhancement in neutral composition at low latitudes as inferred by O(1D) dayglow measurements from Chile, *Ann. Geophys.*, *22*, 3241–3250.

Paxton, L. J., et al. (1999), Global ultraviolet imager (GUVI): Measuring composition and energy inputs for the NASA Thermosphere Ionosphere Mesosphere Energetics and Dynamics (TIMED) mission, *Proc. SPIE Int. Soc. Opt. Eng.*, *3756*, 265–276.

Prölss, G. W. (1976), On explaining the negative phase of ionospheric storms, *Planet. Space Sci.*, *24*, 607–609.

Prölss, G. W. (1980), Magnetic storm associated perturbations of the upper atmosphere: Recent results obtained by satellite-borne gas analyzers, *Rev. Geophys. Space Phys.*, *18*, 183–202.

Prölss, G. W., and S. Werner (2002), Vibrationally excited nitrogen and oxygen and the origin of negative ionospheric storms, *J. Geophys. Res.*, *107*(A2), 1016, doi:10.1029/2001JA900126.

Raghavarao, R., P. Sharma, and M. R. Sivaraman (1978), Correlation of ionization anomaly with the intensity of electrojet, *Space Res.*, *18*, 277–280.

Rajat, A., N. Nagori, N. Jain, S. Sunda, S. Regar, M. R. Sivaraman, and K. Bandyopadhyay (2007), Ionospheric studies for the implementation of GAGAN, *Indian J. Rad. Spa. Phys.*, *36*(5), 394–404.

Rastogi, R. G., and J. A. Klobuchar (1990), Ionospheric electron content within the equatorial F_2 layer anomaly belt, *J. Geophys. Res.*, *95*, 19,045–19,052, doi:10.1029/JA095iA11p19045.

Rishbeth, H., and O. K. Garriot (1969), *Introduction to Ionospheric Physics*, Elsevier, New York.

Rishbeth, H., T. J. Fuller-Rowell, and A. S. Rodger (1987), F-layer storms and thermospheric composition, *Phys. Scr.*, *36*, 327–336.

Roble, R. G., R. E. Dickinson, and E. C. Ridley (1977), Seasonal and solar cycle variations in the zonal mean circulation in the thermosphere, *J. Geophys. Res.*, *82*, 5493–5504, doi:10.1029/JA082i035p05493.

Sastri, J. H. (1988), Equatorial electric fields of ionospheric disturbance dynamo origin, *Ann. Geophys.*, *6*, 635–642.

Sastri, J. H., M. A. Abdu, and J. H. A. Sobral (1997), Response of equatorial ionosphere to episodes of asymmetric ring current activity, *Ann. Geophys.*, *15*, 1316–1323, doi:10.1007/s00585-997-1316-3.

Sastri, J. H., N. Jyoti, V. V. Somayajulu, H. Chandra, and C. V. Devasia (2000), Ionospheric storm of early November 1993 in the Indian equatorial region, *J. Geophys. Res.*, *105*, 18,443–18,455, doi:10.1029/1999JA000372.

Sharber, J. R., R. A. Frahm, R. Link, G. Crowley, J. D. Winningham, E. E. Gaines, R. W. Nightingale, D. L. Chenette, B. J. Anderson, and C. A. Gurgiolo (1998), UARS particle environment monitor observations during the November 1993 storm: Auroral morphology, spectral characterization, and energy deposition, *J. Geophys. Res.*, *103*, 26,307–26,322, doi:10.1029/98JA01287.

Simi, K. G., S. V. Thampi, D. Chakrabarty, B. M. Pathan, S. R. Prabhakaran Nayar, and T. K. Pant (2012), Extreme changes in the equatorial electrojet under the influence of interplanetary electric field and the associated modification in the low-latitude *F* region plasma distribution, *J. Geophys. Res.*, *117*, A03331, doi:10.1029/2011JA01732.

Spiro, R. W., R. A. Wolf, and B. G. Fejer (1988), Penetration of high-latitude electric field effects to low latitude during SUNDIAL, 1984, *Ann. Geophys.*, *6*, 39–50.

Strickland, D. J., R. E. Daniell Jr., and J. D. Craven (2001), Negative ionospheric storm coincident with DE 1-observed thermospheric disturbance on October 14, 1981, *J. Geophys. Res.*, *106*, 21,049–21,062, doi:10.1029/2000JA000209.

Tsurutani, B. T., et al. (2004), Global dayside ionospheric uplift and enhancement associated with interplanetary electric field, *J. Geophys. Res.*, *109*, A08302, doi:10.1029/2003JA010342.

Wang, M., W. Y. Lou, P. Li, X. H. Shen, and Q. Li (2013), Monitoring the ionospheric storm effect with multiple instruments in North China: July 15–16, 2012 magnetic storm event, *J. Atmos. Sol. Terr. Phys.*, *102*, 261–268.

Zhao, B., W. Wan, and L. Liu (2005), Response of equatorial anomaly to the October–November 2003 superstorm, *Ann. Geophys.*, *23*, 693–706, doi:10.5194/angeo-23-693-2005.

Zhao, B., W. Wan, J. Lei, Y. Wei, Y. Sahai, and B. Reinisch (2012), Positive ionospheric storm effects at Latin America longitude during the superstorm of 20–22 November 2003: Revisit, *Ann. Geophys.*, *30*, 831–840.